Marginally-Stable Thermal Equilibria of Rayleigh-Bénard Convection

Liam O'Connor[1], Daniel Lecoanet[1,2], and Evan Anders[2]
[1] *Department of Engineering Sciences and Applied Mathematics, Northwestern University, Evanston, IL 60208 USA and*
[2] *Center for Interdisciplinary Exploration and Research in Astrophysics, Northwestern University, Evanston, IL, 60201 USA*

A novel quasilinear form of the Boussinesq Rayleigh-Bénard equations is derived from the classical linear stability analysis. Eigenfunction amplitudes are obtained by requiring marginal-stability. Symmetric thermally-equilibrated states are then obtained and their properties are analyzed. Such states are compared with statistically-steady 2-dimensional Rayleigh-Beńard convection simulations: marginally-stable thermally-equilibrated states have thinner boundary layers which scale like $\delta \sim Ra^{-1/3}$. 2-dimensional simulations are initialized with solutions to the quasilinear problem; they do not undergo a convective transient period but turn out to be kinetically exaggerated.

I. INTRODUCTION

Rayleigh-Bénard convection plays a foundational role in large-scale astrophysical and geophysical systems. Highly turbulent systems, such as the convective regions of stars, are not well understood. Numerical simulations provide insight into the behavior of convective systems but often times the computational expense is inhibitive. convection is important, particularly rbc; full rbc equations are complicated; simplified models give insight into complicated problem; chini's paper gives interesting new way to develop quasilinear approximation; jklfjakjdfskdjfajlsdjfalskdjflaskjdlfjaljsdklfjlajdlfjaklsjdklfjaljklfjakjdf skdjfajlsdjfalskdjflaskjdlfjaljsdklfjlajdlfjaklsjdklfjaljklfjakjdfskdjfajlsdjfa skdjfajlsdjfalskdjflaskjdlfjaljsdklfjlajdlfjaklsjdklfjaljklfjakjdfskdjfajlsdjfalskdjfajlsdjfalskdjflaskjdlfjaljsdklfjlajdlfjaklsjdklfjaljklfjakjdfskdjfajlsdjfal

II. CONVENTIONAL BOUSSINESQ LINEAR STABILITY ANALYSIS

We begin with the non-dimensionalized Boussinesq approximation for Rayleigh-Bénard Convection. The domain is 2-dimensional rectangular and horizontally periodic with spatial dimensions $0 < x < 4$ and $-1/2 < z < 1/2$. The fluid of interest is constrained between two planar boundaries at $z = -1/2$ and $z = 1/2$ with fixed temperatures 1 and 0 respectively. At both boundaries we specify impenetrable, no-slip conditions, such that the velocity $\mathbf{u} = u\hat{x} + w\hat{z} = \mathbf{0}$ at $z = \pm 1/2$. The equations of motion are then given by

$$\nabla \cdot \mathbf{u} = 0 \tag{1}$$

$$\frac{\partial \mathbf{u}}{\partial t} + \mathbf{u} \cdot \nabla \mathbf{u} = -\nabla p + T\hat{z} + \sqrt{\frac{Pr}{Ra}}\nabla^2 \mathbf{u} \tag{2}$$

$$\frac{\partial T}{\partial t} + \mathbf{u} \cdot \nabla T = \frac{1}{\sqrt{RaPr}}\nabla^2 T \tag{3}$$

where p is pressure and T is temperature. For completeness, we specify a final boundary condition $p = p_0$ at $z = \pm 1/2$. Any system of this form can be characterized by its Rayleigh number Ra and Prandtl number Pr, where Ra is the timescale ratio of thermal diffusion to convection and Pr is the ratio of momentum diffusivity to thermal diffusivity. For convenience, we define

$$\mathcal{R} = \sqrt{\frac{Pr}{Ra}}, \qquad \mathcal{P} = \frac{1}{\sqrt{PrRa}}. \tag{4}$$

To derive the linearized system, we posit that each field can be represented as the sum of a background profile (denoted by $\bar{\cdot}$) and a perturbation function (denoted by $\cdot'$). At an arbitrary time t_0, suppose $\frac{\partial \bar{T}}{\partial z}(z)$ is some given function which satisfies

$$\int_{-\frac{1}{2}}^{\frac{1}{2}} \frac{\partial \bar{T}}{\partial z}\Big|_{t=t_0} dz = -1. \tag{5}$$

Then the background profiles are given by

$$\bar{\mathbf{u}} = \mathbf{0} \tag{6}$$

$$\bar{T}(z) = 1 + \int_{-\frac{1}{2}}^{z} \frac{\partial \bar{T}}{\partial \zeta}\Big|_{t=t_0}(\zeta) d\zeta \tag{7}$$

$$\bar{p}(z) = p_0 - \int_{-\frac{1}{2}}^{z} \bar{T}\Big|_{t=t_0}(\zeta) d\zeta. \tag{8}$$

Accordingly, the fields are defined as

$$\mathbf{u}(x,z,t) = \mathbf{u}'(x,z,t) \tag{9}$$

$$= u'(x,z,t)\hat{x} + w'(x,z,t)\hat{z} \tag{10}$$

$$T(x,z,t) = \bar{T}(z) + T'(x,z,t) \tag{11}$$

$$p(x,z,t) = \bar{p}(z) + p'(x,z,t). \tag{12}$$

Upon substitution, we equate terms which scale linearly with the perturbations, yielding the linearized stability equations

$$\nabla \cdot \mathbf{u}' = 0 \tag{13}$$

$$\frac{\partial \mathbf{u}'}{\partial t} = -\nabla p' + T'\hat{z} + \mathcal{R}\nabla^2 \mathbf{u}' \tag{14}$$

$$\frac{\partial T'}{\partial t} + \frac{\partial \bar{T}}{\partial z} w' = \mathcal{P}\nabla^2 T' \tag{15}$$

with Dirichlet boundary conditions

$$T'|_{z=\pm\frac{1}{2}} = 0, \quad u'|_{z=\pm\frac{1}{2}} = 0, \quad p'|_{z=\pm\frac{1}{2}} = 0. \tag{16}$$

In 1916, Lord Rayleigh observed that (13) and (15) can be manipulated into a separable form with generalized solutions

$$w'(x,z,t) = W(z)\, e^{i(k_x x - st)} \tag{17}$$
$$u'(x,z,t) = U(z)\, e^{i(k_x x - st)} \tag{18}$$
$$T'(x,z,t) = \theta(z)\, e^{i(k_x x - st)} \tag{19}$$
$$p'(x,z,t) = P(z)\, e^{i(k_x x - st)} \tag{20}$$

where $s = \sigma + i\omega$ and k_x is constrained, by periodicity, to the countably infinite set (spectrum) of wavenumbers

$$k_x \in \left\{ \frac{n\pi}{2} \,\middle|\, n \in \mathbb{N} \right\}. \tag{21}$$

For each k_x, we can assess the stability of the perturbations by solving for the eigenvalue s, whose imaginary component ω plays the role of an exponential growth rate. Solution yields a finite set of eigenvalues, among which, that with maximum ω is assumed to be dominant. Positive eigenvalues indicate that the system is unstable to small disturbances of wavenumber k_x, while negative eigenvalues indicate stability. A complete linear stability analysis requires solution over the full spectrum of wavenumbers. The prototypical case is used to demonstrate that the critical Rayleigh number $Ra_c = 1708$ when $\frac{\partial \bar{T}}{\partial z} = -1$.

III. TEMPERATURE PROFILE EVOLUTION

For this investigation, we allow $\bar{T}$ to vary in z and t. Substituting (11) into (3) yields

$$\frac{\partial \bar{T}}{\partial t} + \mathbf{u}' \cdot \nabla T' + \frac{\partial T'}{\partial t} + \frac{\partial \bar{T}}{\partial z} w' = \mathcal{P}\nabla^2 T' + \mathcal{P}\nabla^2 \bar{T}. \tag{22}$$

Subtracting (15) from (22) eliminates several terms. We can replace the advective term $\mathbf{u}' \cdot \nabla T'$ with $\boldsymbol{\nabla} \cdot (\mathbf{u}'T')$ due to (13). Taking the horizontal average of (22), this advective term can be reduced to

$$\frac{1}{4}\int_0^4 \boldsymbol{\nabla} \cdot (\mathbf{u}'T')dx = \frac{\partial}{\partial z}\langle w'T' \rangle \tag{23}$$

where $\langle \cdot \rangle$ denotes the horizontal average. The remaining terms in (22) are unaffected as they are independent of x. The eigenfunctions $W(z)$, $U(z)$, $\theta(z)$, and $P(z)$ do not admit any natural normalization, as (13) - (15) and their subsequent forms are linear with respect to the perturbations. For completeness, we provide the normalization

$$\int_{-\frac{1}{2}}^{\frac{1}{2}} |\theta(z)| dz = 1 \tag{24}$$

and assign each perturbation a yet-unknown amplitude $A \in \mathbb{R}$, thereby allowing us to reduce (22) to the initial value problem (IVP)

$$\frac{\partial \bar{T}}{\partial t} + A^2 \langle w'T' \rangle = \mathcal{P}\frac{\partial^2 \bar{T}}{\partial z^2}, \tag{25}$$

upon which the remainder of this investigation is centered. It is important to keep in mind that the forcing term $\langle w'T' \rangle$ is obtained by solving an eigenvalue problem (EVP) which itself involves $\frac{\partial \bar{T}}{\partial z}$. We also assume this term is composed of eigenfunctions belonging to the dominant mode.

For various Ra and fixed $Pr = 1$, we seek symmetric, marginally-stable temperature profiles $\bar{T}_{eq}(z)$ which are thermally equilibrated, thereby satisfying $\frac{\partial \bar{T}_{eq}}{\partial t} = 0$ according to (25). We employ the `Dedalus` pseudo-spectral python framework to solve the EVP outlined in Section II as well as the IVP (25) by representing each field with a dealiased Chebshev polynomial basis. The necessary number of basis functions varies, as eigenfunctions and temperature profiles associated with large Rayleigh numbers admit increasingly small-scale features. We supplement `Dedalus` with the `Eigentools` package to obtain the eigenfunctions in (25).

To find an equilibrated profile, we begin with a marginally-stable initial profile $\bar{T}_0(z)$ whose construction is outlined in III A. We seek to evolve $\bar{T}_0(z)$ into a new marginally-stable profile $\bar{T}_1(z)$ according to (25) using forward-Euler. This generally involves a unique and unknown value $A^2 > 0$. Our method of finding A^2 is best illustrated through example.

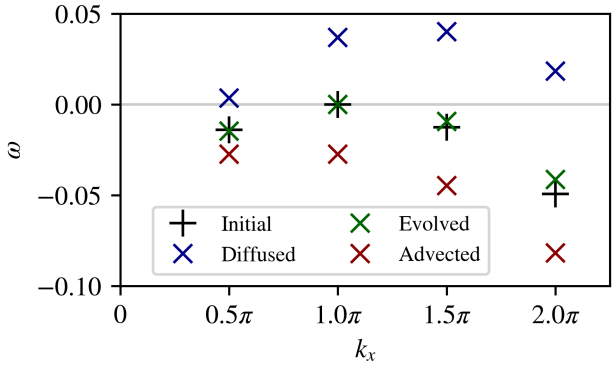

FIG. 1. Eigenvalue spectra for $Ra = 10^5$. The spectrum of a marginally-stable background temperature profile $\bar{T}_0$ (shown in black) has a maximum eigenvalue of 0. Given a small fixed timestep Δt, diffusion destabilizes the system, increasing its eigenvalues (shown in blue). Advection tends to stabilize the system, decreasing its eigenvalues (shown in red). It follows that there exists some proportion (A^2) of these two terms which yields a new marginally-stable background temperature profile $\bar{T}_1$, whose spectrum is shown in green.

An iteration is performed as follows: diffusing a marginally-stable temperature profile $\bar{T}_0$ tends to increase its eigenvalues. Ignoring the diffusive term and

evolving according to advection tends the stabilize the system. The appropriate amplitude A^2 can then be approximated by

$$A^2 \sim -\frac{\omega_{\text{diff}}}{\omega_{\text{adv}}} \tag{26}$$

where ω_{diff} and ω_{adv} refer to the diffused and advected eigenvalues of the initially marginal mode (corresponding to the blue and red points respectively at $k_x = \pi$ in Figure 1). $\bar{T}_0$ is then evolved according to (25) and another eigenvalue solve is performed. Given a fixed timestep Δt, we assume the dominant eigenvalue can be described by a continuous function $\omega_{\max}(A^2)$ which is locally differentiable. Newton's method is used to find an amplitude which meets our marginal stability tolerance criterion $|\omega_{\max}(A^2)| \leq 10^{-9}$. The dominant mode is not fixed; an iteration can facilitate the transfer of marginal-stability from one mode to another. In section III B we specify procedures for the treatment of multiple simultaneously marginal modes.

A. Initial buoyancy profile

In an attempt to minimize the required number of iterations, we initialize with [5]'s analytical thermal boundary layer equation for turbulent Rayleigh-Bénard convection, given by

$$\bar{T}_0(\xi) = \frac{\sqrt{3}}{4\pi}\log\frac{(1+a\xi)^3}{1+(a\xi)^3} + \frac{3}{2\pi}\arctan\left(\frac{4\pi}{9}\xi - \frac{1}{\sqrt{3}}\right) + \frac{1}{4}$$
$$\xi = \frac{z}{\delta_0}, \qquad a = \frac{2\pi}{3\sqrt{3}} \tag{27}$$

where δ_0 is the boundary layer thickness. We expect that each Ra is associated with a unique δ_0 for which $\bar{T}_0(z)$ is marginally-stable. It should be noted that when experimenting with various initial profiles ($\tanh, \text{erf}$, etc.), we obtain indistinguishable equilibrated states, implying that solutions may be unique. An example of (27) is given by the blue curve in Figure 2.

B. Treatment of multiple marginally-stable modes

In most cases, we eventually encounter eigenvalue spectra with multiple simultaneously marginal modes. If ignored, we are forced to reduce the timestep and allow the modes to alternate. Instead, we generalize the advective term in (25) to accommodate N simultaneously marginal modes

$$A^2\langle w'b'\rangle = \sum_{n=1}^{N} A_n^2\langle w'b'\rangle_n \tag{28}$$

where $\langle w'b'\rangle_n$ is composed of perturbations associated with $k_x = \frac{n\pi}{2}$. There are now N amplitudes to solve for and N eigenvalues to keep marginally-stable. In general, we expect a function $\omega : \mathbb{R}^N \to \mathbb{R}^N$ to have isolated roots (should they exist). We employ Broyden's method for root-finding in multi-dimensional functions whose derivatives are not explicitly known. Difficulty arises when transitioning between different numbers of marginal modes. Here we rely on $A^2 > 0$ by asserting that a mode which is *close enough* to marginal-stability can be included in the iteration provided that its respective amplitude is positive. Should we converge upon a negative amplitude, that mode is discarded and the iteration is repeated. In general we find that no other obvious course of action yields equilibria.

IV. PROPERTIES OF THERMALLY EQUILIBRATED STATES

Thermally equilibrated states of this kind are solutions to a particular quasilinear form of the Rayleigh-Bénard convection equations. For this investigation, we calculate solutions for Ra in the range $10^5 - 10^9$. Solutions are symmetric about $z = 0$ by design. This, combined with the fact that we did initialize a background horizontal flow implies the absence of any nonconstant horizontal velocity perturbations.

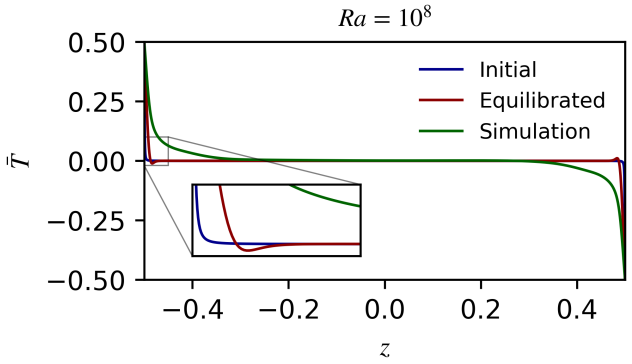

FIG. 2. Background temperature profiles $\bar{T}$ for $Ra = 10^8$. The initial profile is given by (27). The equilibrated curve refers to the background temperature profile of the marginally-stable thermally-equilibrated state. The simulation profile is obtained by performing a 2-dimensional nonlinear simulation with `Dedalus` until thermal and kinetic relaxation. The simulation temperature data are horizontally- and time-averaged. The initial, equilibrated, and simulation profiles have increasingly relaxed boundary regions (respectively). The equilibrated profile exhibits prominent dips, nested alongside the boundary regions. The purpose of this feature is not well understood.

Figure 2 gives temperature profiles for $Ra = 10^8$ where the initial profile, given by (27), is employed at iteration 0; the equilibrated profile corresponds to the thermally relaxed state; and the simulation profile is obtained by performing a nonlinear simulation of (1)-(3)

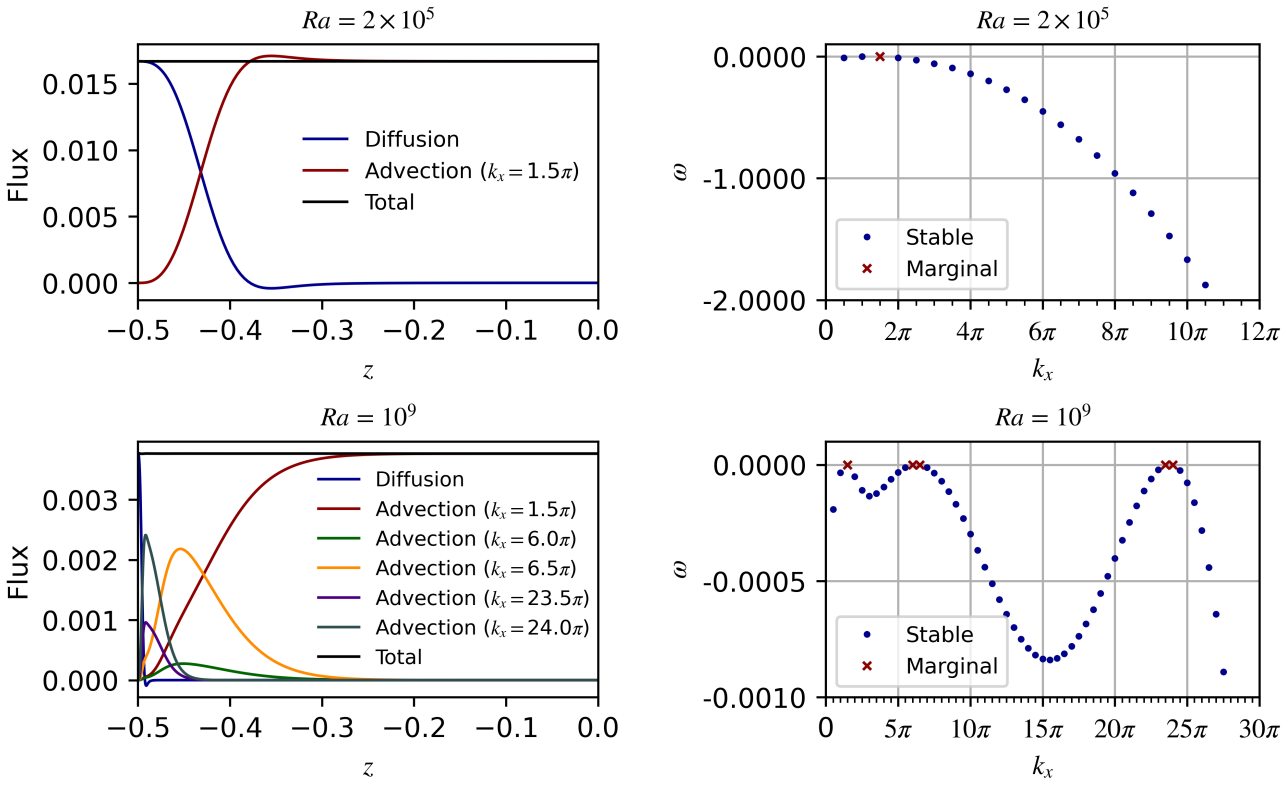

FIG. 3. Heat fluxes (left) and eigenvalue spectra (right) of equilibrated states $Ra = 2 \times 10^5$ (top) and $Ra = 10^9$ (bottom). Advection profiles belong to marginally-stable modes. For low Ra, a single mode with $k_x = 1.5\pi$ is sufficient to oppose boundary layer diffusion and facilitate heat flux throughout the bulk of the domain. For large Ra, high-wavenumber modes contribute pronounced small-scale advection profiles which tightly hug the thin boundary layers. A combination of of progressively wider advection profiles is necessary to transition to the $k_x = 1.5\pi$ mode.

with `Dedalus`, followed by horizontal and time averaging. The simulation curve is more diffuse than the equilibrated curve, which in turn, is more diffuse than the initial curve. Performing an eigenvalue solve by setting $\bar{T}$ equal to the simulation profile yields positive eigenvalues. Comprehensively, this suggests that thermally-equilibrated states might maximize boundary layer thickness, while subject to the marginal stability constraint.

The most resilient and unexpected feature of thermally equilibrated background temperature profiles are the pronounced dips adjacent to the boundary layers. These dips appear in every solution, regardless of Ra. Physically, they correspond to thin layers in which the temperature gradient reverses, contradicting a hypothesis of [1]. This counter-diffusion, which opposes overall heat transfer, is overcome by the coinciding advective flux, shown in Figure 3.

Equilibrated states exhibit distinct behaviors for large and small Ra. This contrast is illustrated in Figure 3, where we give heat flux profiles and eigenvalue spectra for two cases: $Ra = 2 \times 10^5$ and $Ra = 10^9$. For lower Ra, there is a single presumed local maximum in the eigenvalue spectrum, whose adjacent modes' advection profiles occupy the bulk of the domain. These states have relaxed boundary layers which gradually subside as advection becomes the dominant component of the total flux. Such transitional regions do not appear in high Ra cases, where the shift from diffusion to advection is sharp, requiring pronounced, small-scale advection profiles belonging to modes adjacent to the third presumed local maximum in the eigenvalue spectrum. Traversing towards the midplane of the domain, we see increasingly thicker advection profiles corresponding the wavenumbers adjacent to the second local maximum, eventually culminating in the dominant $k_x = 1.5\pi$ mode.

Thermally equilibrated states with large Ra tend to have a more diverse set of marginal modes as compared to small Ra states. In every case, the $k_x = 1.5\pi$ mode is included and is often unaccompanied by adjacent modes. In Figure 4 we give the wavenumbers k_x of marginal modes, color coded accordingly to their respective adjacencies. Marginal modes often appear in neighboring pairs, in which case the larger mode is denoted with an x and the smaller mode is denoted with a +. In these cases we infer the existence of a local maximum eigenvalue between the two adjacent marginally-stable modes. For $Ra \geq 10^6$, a second branch of marginal modes is introduced as shown in green, increasing according to some

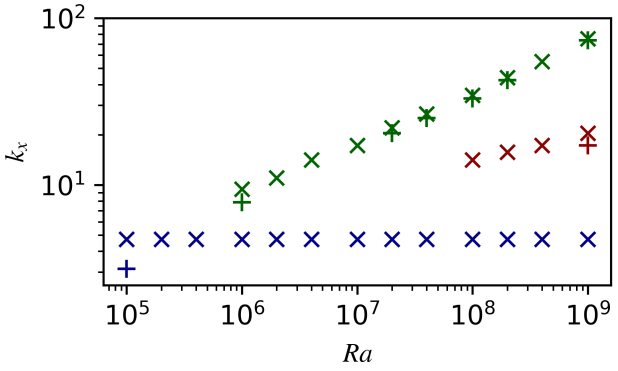

FIG. 4. Wavenumbers of marginally-stable modes of thermally equilibrated states. Markers are color-coded according to their adjacent local maxima index in the eigenvalue spectrum. For example, the spectrum corresponding to $Ra = 10^5$ has marginal wavenumbers $k_x = \pi$, 1.5π adjacent to a presumed local maximum between these two allowed values. The $Ra = 10^9$ spectrum, shown in lower right corner of Figure 3, has three presumed local maxima, with a single marginal mode adjacent to the first maximum ($k_x = 1.5\pi$), two marginal modes adjacent to the second maximum ($k_x = 6\pi$, 6.5π), and two marginal modes adjacent to the third maximum ($k_x = 23.5\pi$, 24π). The largest wavenumbers of the green branch obey a power-law relationship with Ra

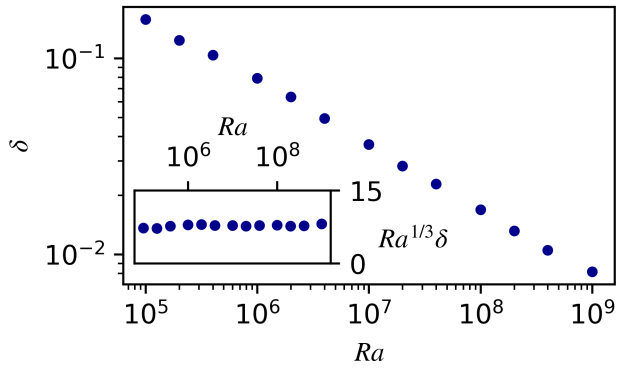

FIG. 5. Boundary layer widths δ of marginally-stable thermal equilibria. We define the threshold of each boundary layer as the z-coordinate at which $\frac{\partial \bar{T}}{\partial z} = 0$, corresponding to the local extrema of the equilibrated curve in Figure 2. Plotting on a log-log scale, we find δ and Ra obey a power-law relationship. We also demonstrate that $Ra^{1/3}\delta$ is approximately constant with respect to Ra implying $Ra \propto \delta^{-3}$, as predicted by [1]

power-law with respect to Ra. The introduction of this largest branch is likely required to oppose the diffusion of the thinning boundary layers. For $Ra \geq 10^8$, a third branch appears (shown in red), splitting the widening gap between the blue branch and the green branch. This development is associated with relatively thick advection profiles, filling a niche in the total flux by uniting the sharp profiles of the largest branch (green) and those of the bulk-domain-oriented smallest branch (blue).

In general, marginally-stable thermal equilibria can be characterized by their boundary layer thicknesses, from which, the rest of their properties follow. Letting the interior boundary layer threshold be the z-coordinate at which $\frac{\partial \bar{T}}{\partial z} = 0$, we find that $Ra \propto \delta^{-3}$ as illustrated in Figure 5. This is consistent with Malkus' marginal-stability theory, a scaling argument which perceives the boundary regions as subdomains which are themselves marginally-stable.

Nusselt numbers Nu of various solutions are given in Figure 7. The marginally-stable thermally-equilibrated states and numerical simulation data exhibit power-law relationships with Ra. More specifically, $Ra \sim Nu^3$ which agrees with Figures 5, 4, and 6 and the scaling argument given by [1]. The nonlinear solutions, which maximize heat flux, are obtained [7]. Nu of both equilibria exceed that of simulations, which might be due to the transitional behaviors outlined by [8] inhibitting heat flux.

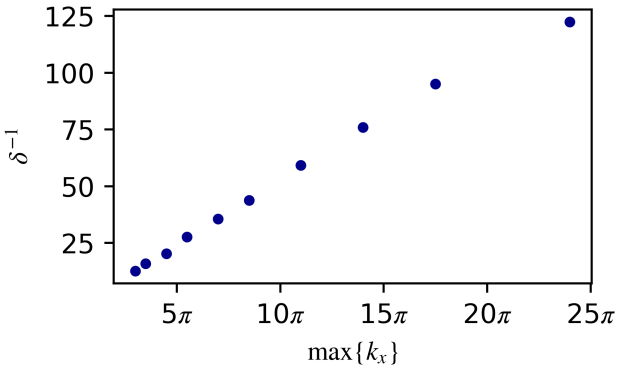

FIG. 6. For $Ra \geq 10^6$, the maximum marginally-stable wavenumber (corresponding to the green X markers in Figure 4) are inversely related to the boundary layer thicknesses δ. $(\max\{k_x\})^{-1}$ gives a minimum x length scale for the perturbations, and consequently, the advection. We expect the minimum z length scale to agree with the boundary layer thickness δ because otherwise the boundary layer would continue to diffuse. This is well illustrated in the lower left corner of Figure 3, where the advection profile for $k_x = 24\pi$ is tightly flanked by the surrounding boundary layers. This suggests that the minimum x and z length scales obey some constant ratio.

V. SIMULATIONS WITH THERMALLY EQUILIBRATED INITIAL CONDITIONS

This investigation is partially motivated by the prospect of decreasing nonlinear simulation relaxation times by employing thermally-equilibrated initial conditions. Conventionally, (1) - (3) are solved via direct nu-

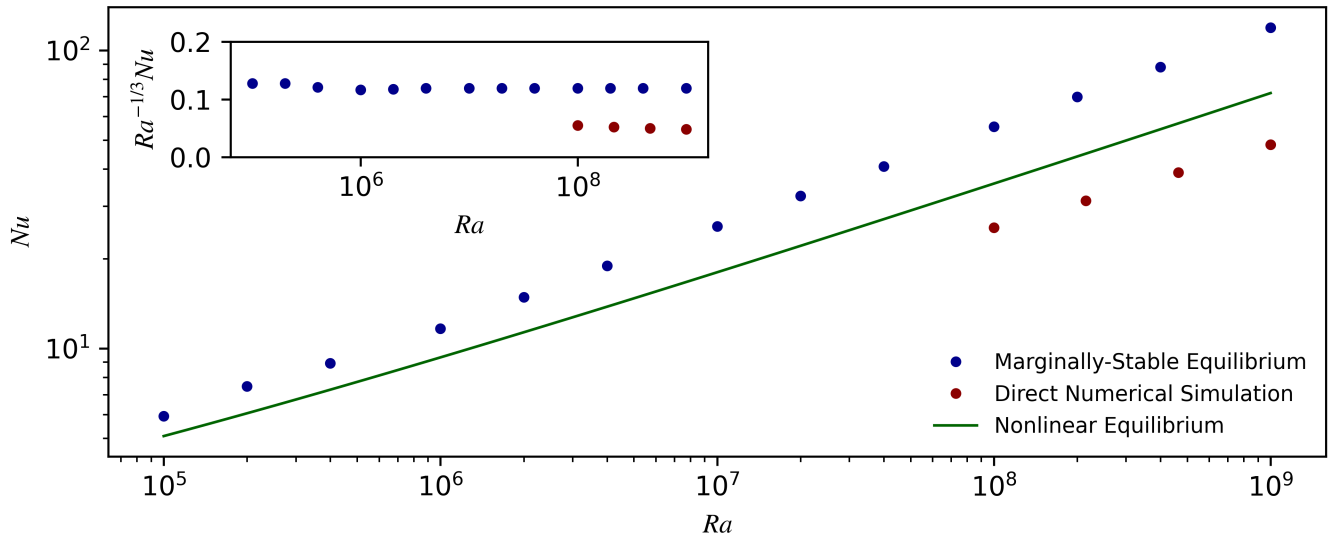

FIG. 7. Nusselt numbers are shown for marginally-stable thermally-equilibrated states, statistically-steady direct numericals simulations performed with `Dedalus` [6], and equilibrated nonlinear solutions, which maximize heat flux, given by [7]. Both obey power-law relationships with Ra, with $Ra \sim Nu^3$ in agreement with Figures 5, 4, and 6 as well as [1]. Marginally-stable states' Nusselt numbers exceed simulation Nusselt numbers. This can be well explained by the contrasting boundary region geometries shown in Figure 2.

merical simulation (DNS) with initial conditions

$$T(x,z)\big|_{t=0} = 0.5 - z \tag{29}$$
$$\mathbf{u}(x,z)\big|_{t=0} = \mathbf{0} \tag{30}$$
$$p(x,z)\big|_{t=0} = 0 \tag{31}$$

which will hereby be referred to as the conductive initial condition. t in this section now refers to the simulation time as opposed to the thermal equilibration time parameter used previously. We define the equilibrated initial conditions

$$T(x,z)\big|_{t=0} = \bar{T}(z) + \sqrt{2}\sum_{n=1}^{N} A_n \,\mathrm{Re}\Big[\theta_n(z) e^{ik_{x_n}x}\Big]$$
$$\mathbf{u}(x,z)\big|_{t=0} = \sqrt{2}\sum_{n=1}^{N} A_n \,\mathrm{Re}\Big[\Big(U_n(z)\hat{x} + W_n(z)\hat{z}\Big) e^{ik_{x_n}x}\Big]$$
$$p(x,z)\big|_{t=0} = \sqrt{2}\sum_{n=1}^{N} A_n \,\mathrm{Re}\Big[P_n(z) e^{ik_{x_n}x}\Big] \tag{32}$$

Where $\theta_n(z), U_n(z), W_n(z), P_n(z)$; A_n; and k_{x_n} refer to the complex eigenfunctions, amplitude, and wavenumber at the nth marginal mode. The $\sqrt{2}$ factor is necessary for eigenfunction normalization. By construction, these initial conditions are thermally equilibrated. Simulations launched with equilibrated initial conditions do not exhibit a convective-transient period, as the large-scale anatomy of plumes and convective winds which are characteristic of Rayleigh-Bénard convection exist on initialization. This is illustrated in Figure 8, where the

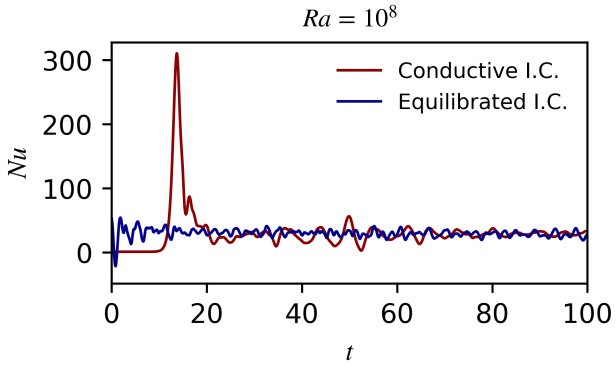

FIG. 8. Nusselt numbers of simulations performed at $Ra = 10^8$ with conventional initial conditions (red) and marginally-stable thermally-equilibrated initial conditions (blue). Simulations launched with thermally-equilibrated states do not undergo a convective-transient period because the characteristic plume structure exists on initialization. This is illustrated by the Nu spike at $t \sim 15$ in the convectional simulation.

sharp spike in Nu is associated with a turbulent transitional period of upwelling until the distinctive jet-like structure is established.

The marginally-stable equilibria are associated with a combination of eigenfunctions whose average kinetic energy is significantly larger than the statistical steady state, as given by Figure 9. This is postpones kinetic relaxation because the large horizontal flows decay on a

viscous timescale

$$t_\nu \sim \sqrt{\frac{Ra}{Pr}}.$$

Consequently, marginally-stable thermally-equilibrated initial conditions do not reduce the simulation time required to achieve a statistically steady state, rather, they increase it considerably.

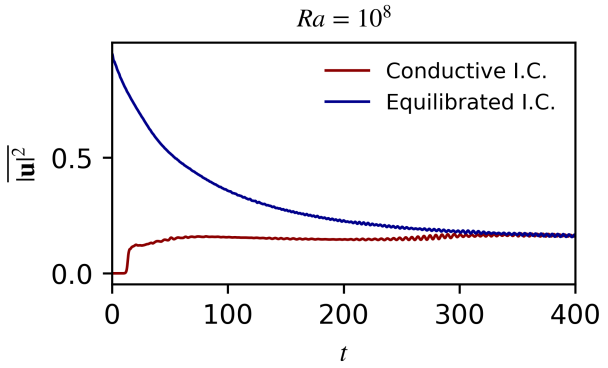

FIG. 9. Average kinetic energies of the same simulations performed in Figure 8 ($Ra = 10^8$). The combination of eigenfunctions which give thermal equilibrium have significantly more kinetic energy than the statistically steady state. Kinetic equilibrium is achieved according to the viscous timescale $t_\nu \sim PrRa^{-1/2}$.

VI. CONCLUSION

APPENDIX

This is an appendix

ACKNOWLEDGMENTS

Jeff Vassil, Greg Chini,

[1] Malkus W. V. R. 1954 The heat transport and spectrum of thermal turbulenceProc. R. Soc. Lond. A225196–212
[2] Howard L.N. (1966) Convection at high Rayleigh number. In: Görtler H. (eds) Applied Mechanics
[3] Chini, G., Malecha, Z., & Dreeben, T. (2014). Large-amplitude acoustic streaming. Journal of Fluid Mechanics, 744, 329-351. doi:10.1017/jfm.2014.61
[4] Michel, G., & Chini, G. (2019). Strong wave–mean-flow coupling in baroclinic acoustic streaming. Journal of Fluid Mechanics, 858, 536-564. doi:10.1017/jfm.2018.785
[5] Olga Shishkina, Susanne Horn, Sebastian Wagner, Phys. Rev. Lett. 114
[6] Evan H. Anders, Geoffrey M. Vasil, Benjamin P. Brown, and Lydia Korre Phys. Rev. Fluids 5, 083501
[7] Waleffe F., Boonkasame A., Smith L.M. Heat transport by coherent Rayleigh–Bénard convection Phys. Fluids, 27 (2015), Article 051702
[8] Coarse graining the state space of a turbulent flow using periodic orbits Yalnız, Gökhan; Hof, Björn; Burak Budanur, Nazmi